

**AIRIS HYPERSPECTRAL IMAGING TECHNOLOGY**

Christopher M. Gittins\* and William J. Marinelli†  
 Physical Sciences Inc.  
 Andover, MA 01810-1077

Anthony J. Ratkowski‡  
 USAF Phillips Laboratory PL/GPO  
 Hanscom AFB, MA 01731-3010

Abstract

The Adaptive InfraRed Imaging Spectroradiometer (*AIRIS*) is a hyperspectral imaging system comprising a low-order tunable Fabry-Pérot étalon coupled to an IR focal plane array. A MWIR *AIRIS* system utilizing an InSb focal plane was developed by Physical Sciences Inc. (PSI) under the sponsorship of the Armament Division, Air Force Wright Laboratories for high-speed multispectral imagery of countermeasures and missile systems. The system has been transferred to PSI under a bailment agreement and is currently being used in a joint effort with the Geophysics Directorate of the Air Force Phillips Laboratory to examine the utility of multispectral imagery for strategic and tactical applications. In this paper we discuss: 1) the underlying concepts which form the basis of the *AIRIS* sensor, 2) implementations of the concept and methods for optimizing system performance, 3) laboratory and limited field data gathered by MWIR variant of the sensor, and 4) preliminary data from an LWIR system under development. A key feature of the *AIRIS* approach is the ability to rapidly image the scene at only those wavelengths needed for identification and clutter suppression. This capability reduces the data rate, data volume, and processing requirements needed to effectively employ hyperspectral imagery for these applications.

Introduction

The Adaptive Infrared Imaging Spectroradiometer (*AIRIS*) is an innovative imaging, piezoelectrically

\*Principal Scientist

†Principal Research Scientist, AIAA Member

‡Senior Advisor, Optical Effects Div., AIAA Member

actuated Fabry-Pérot interferometer originally developed under BMDO and Air Force sponsorship by Physical Sciences Inc. (PSI). The distinguishing feature of the approach is the operation of the interferometer in low orders such that continuous, narrow spectral bandwidth images are produced over a wide field-of-view. A computer is used to control mirror spacing, alignment, and processing of the infrared images and a staring focal plane array captures an image of the interferometer field-of-view with high sensitivity.

Beneficial features of the low-order interferometer based imaging system include: 1) an extended free spectral range (up to  $\lambda$  to  $2\lambda$ ), 2) a narrow spectral bandwidth (approximately 2% of  $\lambda$ ), 3) flexible and adaptive sampling and processing of the image to isolate specific spectral features or signatures, 4) high spatial resolution and radiance sensitivity, 5) a common pixel registry for all detection wavelengths, and 6) an extended field-of-view (as great as 40 deg full angle) for the survey of wide areas.

The aforementioned features are incorporated into a compact device which can provide full spectral coverage of the SWIR, MWIR, or LWIR atmospheric transmission windows at a spectral resolution consistent with the detection of structured molecular absorption or emission bands. These capabilities allow for the isolation of vehicle plume emissions across several bands, the detection of camouflaged targets in a cluttered environments, as well as the observation and limited quantification of absorption or emission from specific airborne hazardous chemicals in the presence of spectrally structured and cluttered backgrounds. Typical scenarios include:

Approved for public release; distribution is unlimited.

**DTIC QUALITY INSPECTED**

19970912 138

- Detection of aircraft, cruise missiles, and theatre ballistic missiles in both the 4.3 and 2.7  $\mu\text{m}$  bands, from ground, UAV, aircraft and space platforms;
- Imaging and quantification of battlefield chemical agent plumes and damage assessment of chemical production facilities;
- Monitoring of facilities relevant to treaty compliance;

In this paper we report on: 1) the underlying concepts which form the basis of the *AIRIS* sensor, 2) implementations of the concept as well as methods for optimizing system performance, 3) laboratory and limited field data gathered by MWIR variants of the sensor, and 4) preliminary data from an LWIR system under development. The paper presents field observations made with the MWIR system conducted under a joint effort between PSI and PL/GPO at Hanscom AFB.

#### Low Order Imaging Fabry-Pérot Interferometry

The *AIRIS* instrument comprises an IR focal plane array (FPA) coupled to a Fabry-Pérot interferometer through imaging optics. In this configuration the interferometer operates as a tunable interference filter, selecting the wavelength viewed by the FPA. In this section we describe the theoretical basis for the development of the interferometer as well as the consequences and advantages of low-order operation.

In a Fabry-Pérot interferometer, light is selectively transmitted by constructive interference through the faces of two partially-reflecting parallel mirrors. Light is transmitted for wavelengths which satisfy the resonance condition:

$$2\ell \cdot \cos\theta = \left[ m + \frac{\epsilon(\lambda)}{\pi} \right] \cdot \lambda \quad (1)$$

where

- $\ell$  = mirror spacing
- $\theta$  = incidence angle
- $\epsilon(\lambda)$  = phase change upon reflection
- $m$  = order of interference
- $\lambda_t$  = transmitted wavelength.

A range of mirror spacings, incidence angles, and

orders will all lead to the transmission of a single wavelength. The **free spectral range**,  $\Delta\lambda_{\text{FSR}}$ , determines the range of wavelengths transmitted between successive orders of interference. If reflected phase dispersion is neglected, then the free spectral range may be approximated as:

$$\Delta\lambda_{\text{FSR}} = \frac{\lambda_{\text{max}}}{m_{\text{max}} + 1} \quad (2)$$

where  $m_{\text{max}}$  is the order in which  $\lambda_{\text{max}}$  is transmitted for paraxial rays.

The **finesse**,  $F$ , determines the spectral resolution of the interferometer, which is always a fraction of the free spectral range:

$$\Delta\lambda_{1/2} = \frac{\Delta\lambda_{\text{FSR}}}{F} \quad (3)$$

The elements which define the finesse of the interferometer arise from the reflectivities of the mirrors as well as "defects" in their configuration, such as mirror flatness and parallelism. The total finesse of the interferometer is obtained from the inverse root mean square sum of each finesse component. For practical operation in the infrared, the defect finesse is the limiting factor in determining total finesse. The total finesse can seldom be greater than approximately 30 to 50 due to these limitations. We have developed a novel alignment technique employing a digital high speed variant of capacitance micrometry which can achieve mirror spacings with an accuracy of  $6 \times 10^{-3} \mu\text{m}$ . Hence, mirror parallelism is seldom a limitation in the overall finesse of the system.

The interferometer field of view (focal length and detector element size) determine the range of angles incident and detected by the system. Equation (1) shows that a range of incidence angles and interference orders will allow transmission of a common wavelength through the interferometer for a single mirror spacing. This relationship leads to the observation of a central spot, surrounded by a series of concentric rings (Airy pattern), when the interferometer is used to view a

monochromatic source. The relationship is quantified

by the expression:

$$\theta_n = \cos^{-1} \left[ \frac{(m_{\max} - n)}{m_{\max}} \right] \quad (4)$$

where  $\theta_n$  is the angle of incidence (with respect to paraxial rays) from which ring,  $n$ , originates. In conventional high order operation  $m_{\max} \gg n$  and thus the concentric ring pattern is observed over a very narrow range of acceptance angles. In low order operation  $m_{\max} \approx n$ , the first ring occurs at a large value of  $\theta_n$ , and thus a system with a modest acceptance angle views only the central spot in the Airy pattern which contains a continuous monochromatic image of the scene.

The useful range of angles within the central spot is determined by the spectral resolution requirement for the system. The **aperture finesse** defines the degradation in spectral resolution within the central spot as a function of the order,  $m_{\max}$ , and system acceptance angle,  $\Delta\theta$ :

$$F_A = \frac{2}{m_{\max}(\Delta\theta)^2} \quad (5)$$

$\Delta\theta$  = half angle FOV in radians

As a consequence of Eq. (5), the field of view over which an acceptable finesse can be obtained increases as the interferometer is operated in lower orders. When using IR focal plane arrays, system instantaneous fields-of-view ranging from 6 to 15 deg are generally consistent with an overall finesse of 35. If external FOV scanning elements such as galvanometers are employed, the Field of Regard can be expanded to as great as 40 deg with no impact on spectral resolution. The innovative combination of an expanded free spectral range coupled with a wide field of view for low order operation of the interferometer is the focus of U.S. Patent 5,461,477 granted to Physical Sciences Inc.

#### Operational Considerations

In contrast to typical thermal imagers, which may have spectral bandwidths of 2 to 4  $\mu\text{m}$ , the high spectral resolution of the Fabry-Pérot imaging spectroradiometer limits the amount of light from the farfield incident on the detector. A consequence of the reduc-

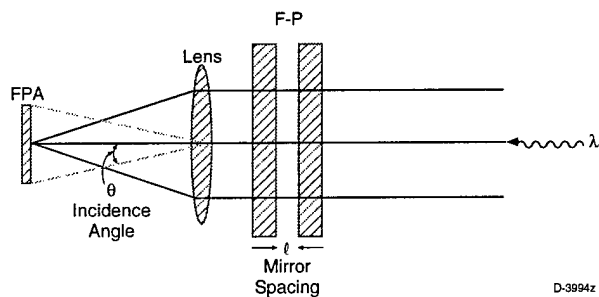
tion in spectral bandwidth is that light originating from the nearfield optics, such as the imaging lens, interferometer mirrors and their enclosures, plays a more important role in determining the total intensity incident on the detector. A significant improvement in system performance can be obtained if the optics and their cavity are cooled to reduce their thermal radiation incident on the detector. The temperature and extent to which the optics must be cooled is a function of the detector, optics, free spectral range, and viewing geometry. Our efforts to mitigate these effects will be discussed later in the paper.

The use of focal plane arrays (as opposed to scanning single element detectors) also offers a significant improvement in performance. The primary benefit arises from the reduction in signal bandwidth which ensues from the ability to stare at a single point in space for the entire framing time. In most viewing scenarios the photon flux from the scene over the small wavelength interval sampled, compared to the inherent read noise in the FPA, determines the signal quality. If self radiance in the imager is carefully managed, such that the detector charge wells are not filled by the near field optics, the framing time is typically controlled by the radiant intensity and the characteristic time of motion in the scene.

#### MWIR Imaging Interferometer Configuration

Two configurations of the imaging system operating in the MWIR have been developed, with additional systems currently under design and construction. One system utilizes a Cincinnati Electronics IRC-160, 160 x 120 InSb focal plane array with a tunable Fabry-Pérot having tube-type piezoelectric mirror actuators. A second system consists of an Amber 5128C, 128 x 128 InSb FPA and an interferometer with "inchworm" piezoelectric-based stepper motor mirror actuators (Burleigh, Fishers, NY). The latter system, recently used to acquire multispectral imaging data at Hanscom AFB, is described below.

A concept diagram of the AIRIS optical system is shown in Figure 1 and a recent version of the MWIR imager is shown in Figure 2. A commercially available Amber 5128C 128 x 128 InSb focal plane array (FPA) capable of framing at 1000 Hz is coupled to the Fabry-Pérot tunable filter module using a 50 mm focal length



D-3994z

Figure 1. Basic configuration for PSI's imaging spectroradiometer systems.

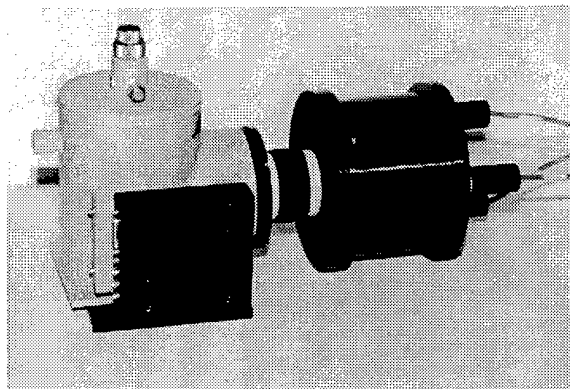


Figure 2. Basic imager concept showing interferometer, imaging lens, and focal plane array.

f/2.3 three element lens assembly to provide image acquisition. A version of this *AIRIS* system, *AIRIS-DF*, was recently delivered to the Air Force Wright Laboratories Armament Division. This system is unique in that it accepts simultaneously, two orders of interference transmitted by the interferometer (2 and 3) and directs them, using dichroic optics, on to separate halves of the 128 x 128 FPA to broaden the wavelength coverage of the system while maintaining high spectral resolution.

Using a dedicated 286-processor based interferometer control system interfaced to a four-channel Amber ProView system with 8 megapixels of memory, we have been able to obtain 128 x 128 hyperspectral images at a rate of approximately 165 frames per second. The capacitance micrometry system is unique in that it is entirely digital. The dedicated 286

processor provides active control of mirror spacing and alignment of the interferometer as well as the process of image acquisition with the FPA. The ProView image acquisition system is run on a 486 processor-based host computer. The system is completely compatible with ruggedized industrial PC's for field use. The control systems for *AIRIS* devices under construction utilize plug-in cards on a Pentium-processor based PCI bus. Custom software routines allow the synchronization of image acquisition with interferometer mirror motion, all on the same processor platform. Data processing uses the Interactive Data Language (IDL) from Research Systems Inc. We have developed routines under Microsoft C++ which allow the imager control system to function under Windows 3.1 as a DLL. This advance allows the control routine to be called directly from IDL, making possible adaptive analysis and acquisition of data.

*AIRIS* interferometer optics are kept at ambient temperature. A cold filter, which selects the interferometer transmission order illuminating the FPA, is incorporated into the FPA dewar and held at the 77 K temperature of the focal plane. We have been successful in reducing the self radiance of the optics by cooling the imaging lens assembly, which is typically focussed at infinity, while maintaining the interferometer at ambient temperature. Cooling of the lens assembly is accomplished thermoelectrically, by sealing it in a hermetic enclosure equipped with a water cooled heat exchanger. This configuration preserves the ability to adjust the focus while the lens is cold. The interferometer mirrors reflect all non-resonant wavelengths. Thus, system self radiance is comprised of the radiance from the FPA (77 K) reflected back onto itself summed with self-radiance and scattering from the imaging lens assembly. The impact of the cooled imaging lens is to reduce the self radiance of the lens assembly in direct proportion to it's blackbody temperature. Supporting data is shown in Figure 3. The centerline radiance for a system viewing an LN<sub>2</sub>-cooled plate is plotted as a function of lens temperature. The expected behavior for a unit emissivity blackbody is shown for comparison. The data clearly show a factor of ~5 reduction in self radiance of the system when the lens temperature is dropped from 24°C to -15°C. The use of lens cooling allows us to increase the FPA integration time while avoiding saturation. The flatness of the field in the system is further improved through the use of an f/3.4 cold shield on the FPA. This improvement is derived at the expense of a factor of 2 in throughput. This

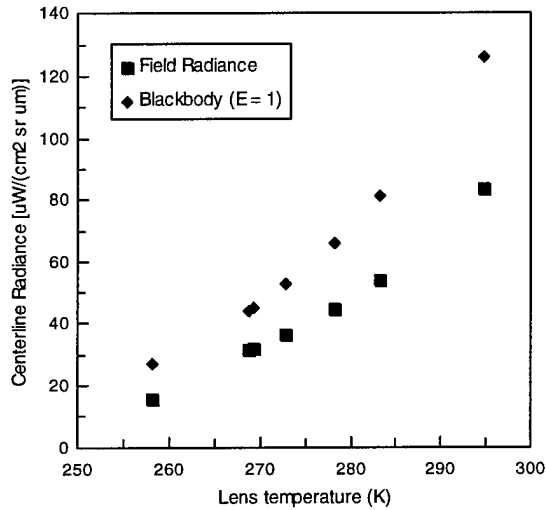


Figure 3. Apparent field radiance and calculated blackbody radiance as a function of lens assembly temperature.

approach is applicable to many commercially available InSb FPA's, allowing us to adapt these to multispectral imaging applications.

Performance Characteristics

Three key performance characteristics for the AIRIS system are spectral resolution, out of band rejection, and radiant sensitivity. The spectral resolution of the system was measured by placing the interferometer in the cavity of an FTIR spectrometer. A sample spectrum is shown in Figure 4, which includes a fit to

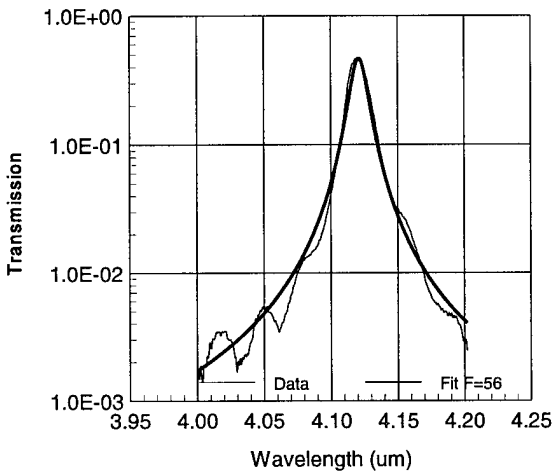


Figure 4. Spectral resolution function for MWIR spectrometer measured using FTIR.

an Airy function - the expected lineshape. The experimental spectrum is consistent with a finesse of 56 (spectral resolution of 0.015  $\mu\text{m}$ ). The lineshape indicates a maximum filter transmission of 60% and a minimum in the filter transmission of  $2 \times 10^{-3}$ . The geometrical throughput for the system with the Amber 5128C FPA ( $f/3.4$  cold shield, 50  $\mu\text{m}$  pixel pitch, 50 mm focal length optics) is approximately  $3 \times 10^{-2} \text{ cm}^2 \text{ sr}$  for the entire array. Thus, the system is capable of very high overall light gathering ability. The AIRIS system is calibrated radiometrically using a two-temperature blackbody approach for each pixel at each wavelength. The average radiant sensitivity of the AIRIS-DF system delivered to Wright Laboratories at 34.5°C is shown in Figure 5. The data shows an average noise-equivalent spectral radiance (NESR) of 1.5  $\mu\text{W}/(\text{cm}^2 \text{ sr } \mu\text{m})$  at a framing rate of 160 per second.

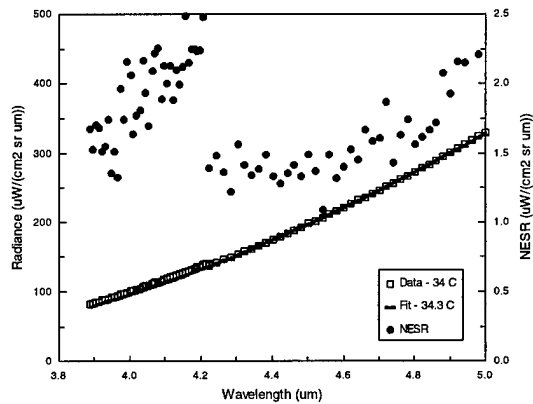


Figure 5. Radiance calibration and NESR for AIRIS-DF system at 34.3°C.

Examples of Imaging Interferometer Applications

Ambient temperature Scenes

In the MWIR, the system operates at mirror separations from  $\sim 6$  to  $\sim 7 \mu\text{m}$  ( $m = 3$ ; the precise spacing is difficult to determine as reflected phase dispersion in the MWIR mirror coating is known only to moderate accuracy) with a cold bandpass filter positioned over the FPA to restrict the response to the free spectral range of 4.05 to 4.75  $\mu\text{m}$ . In this spectral region thermal signatures, solar and thermal reflections, and spectral signatures from hot gases can all be observed.

AIRIS has been used to observe a variety of scenes both in the laboratory and in the field. Hot gases and

spectral lines were used to test resolution and provide laboratory simulations. Full spatial/ spectral data sets of several different types of clouds and aircraft have been acquired. An example of a vehicle located in wooded terrain is presented in Figure 6 for a standoff distance of 100 meters. This scene, viewed through *AIRIS*, is a 7 x 9 deg image at 4.66  $\mu\text{m}$  ( $\pm 0.008 \mu\text{m}$ ). In the scene, an automobile is parked on the shoulder of a curved road. A grassy field is in the foreground, with trees behind. Individual tree trunks can be observed in the original data. A clear undistorted image is obtained across the entire field of view of the monochromatic scene. Solar glint is observed on the automobile rear window. The tires (and even the tailpipe) are discernable. Heat reflected from the gravel under the operating engine is clearly observed. As the transmission wavelength is swept over the 4.1 to 4.8 range, the contrast and relative brightness of different objects in this scene vary. These spectral differences permit roads, trees, grass, and vehicles to be spectrally identified and processed automatically to catalog scene content and highlight regions of interest. Figure 7 shows the spectrum of the reflected engine radiance region of the base of the car. This spectrum was compiled from 28 discrete images of the scene at 0.02  $\mu\text{m}$  separation.

Combustion/Exhaust Gasses

The dual field imaging built for Wright Laboratories, *AIRIS-DF*, was optimized for the observation of countermeasures (flares) and missile exhaust plumes. In the laboratory these sources are simulated using road flares or propane torches. An example imagery from such data is shown in Figure 8 for the observation of a

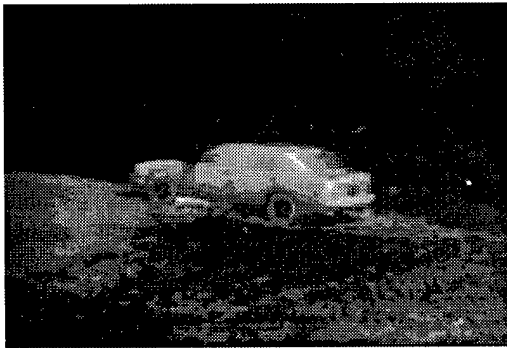


Figure 6. Image of automobile in treed scene at 4.66  $\mu\text{m}$ .

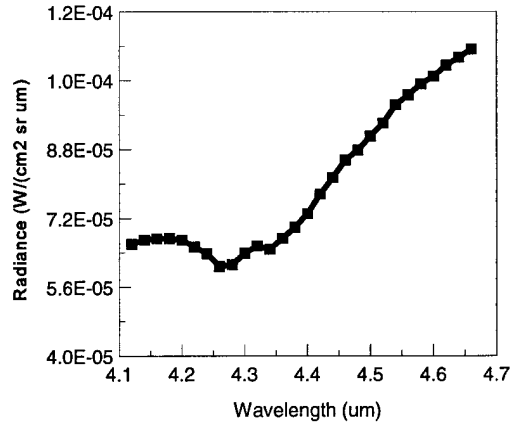


Figure 7. *AIRIS* spectrum from base region of automobile.



Figure 8. Propane torch image at 4.48  $\mu\text{m}$  using CE IRC-160 FPA.

propane torch at a range of 2 meters. (The image displayed in Figure 6 was recorded using the Cincinnati Electronics IRC-160 FPA described earlier.) The FPA integration time is reduced to eliminate saturation in the flame region. As a result of the reduced sensitivity, emission from the scene background falls below the detection limit. The scene is viewed at 80 discrete wavelengths over the range from 3.80 to 4.95  $\mu\text{m}$ . The spectrum of the region at the base of the torch is shown in Figure 9. The calibrated spectrum clearly shows the  $\text{CO}_2$  emission from the flame region, as modified by the 4.3  $\mu\text{m}$  atmospheric absorption band.

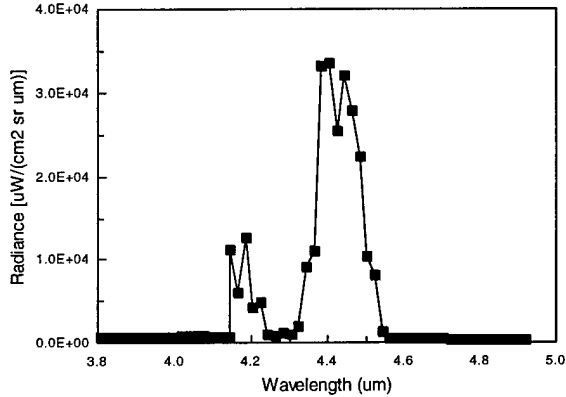


Figure 9. Spectrum of base region of propane torch.

Field Observations of Propane Torch

The AIRIS system has been used to detect similar emission spectra in cluttered scenes. In this paper we report on preliminary data employing a simple correlation analysis to use spectral signatures to identify the hot CO<sub>2</sub> plume originating from a propane torch. A broadband infrared image of the test scene is shown in Figure 10, with a comparable IR image of the scene, recorded at 4.56 µm, shown in Figure 11. The location of the torch in the scene is somewhat evident in the IR image. From the spectral/spatial data cube of this scene we extracted feature spectra of various elements in the scene. Examples are shown in Figure 12 for the



Figure 10. Broadband IR image of scene containing propane torch used in correlation analysis.



Figure 11. Narrow-band IR image at 4.52 µm of scene containing propane torch.

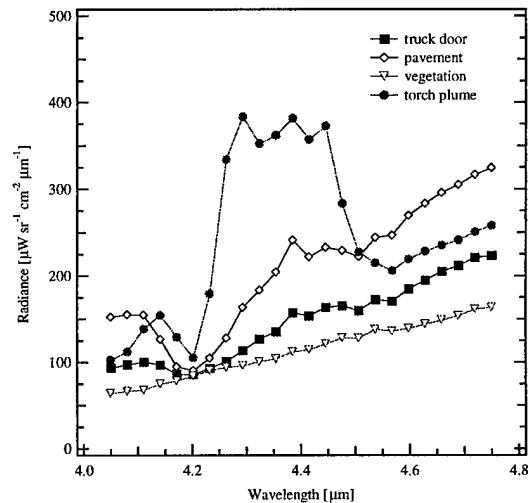


Figure 12. Feature spectra of various scene elements recorded using MWIR AIRIS imager.

torch, asphalt pavement, automobile side, and treed background. These spectra show a clear difference between these various surfaces. (The preliminary spectra in Figure 12 are offset 0.1 µm to shorter wavelengths due to calibration changes resulting from a soft mechanical coupling between the inchworm actuators and one of the interferometer mirror mounts. The problem is understood and is currently being remedied.) This data was used to conduct a two band correlation analysis using 4.05 and 4.41 µm images. The goal of the analysis was to isolate the spatial region containing the torch in the scene. The correlation

analysis is shown in Figure 13. The data was fit using a linear least squares analysis to define the characteristics of the background. Points lying outside the  $5\sigma$  error limits are then plotted as black points on a gray field in Figure 14 to reveal the location of the torch in the scene, isolated from other scene clutter. We are currently working on additional data acquisition and analysis approaches to improve the ability to detect much weaker sources against comparably cluttered scenes.

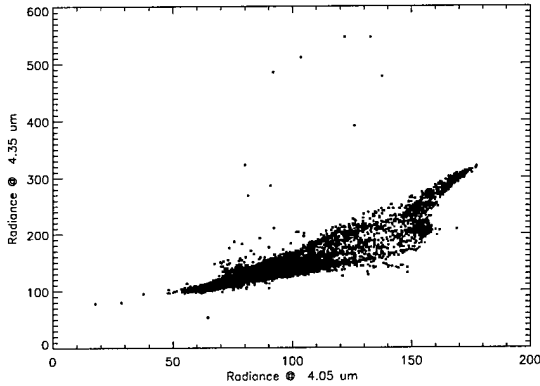


Figure 13. Two band correlation plot for IR imagery containing hot CO<sub>2</sub> plume. Pixels containing CO<sub>2</sub> emission fall well above the primary point cluster.



Figure 14. Broadband IR image with location of hot CO<sub>2</sub> plume identified by correlation analysis.

### Wildfire Imaging

Airborne multispectral imaging systems are employed by NASA and the USDA Forest Service for the mapping and management of wildfires. This application requires that the sensor system have high dynamic range in radiance and precise registration of the imagery with respect to ground features. The MWIR *AIRIS* system is being incorporated into an airborne system for the mapping of wildfires as well as the analysis of plume composition. Preliminary data acquired on a test burn is shown in Figures 15, 16, and 17. In Figures 15 and 16 we show images of the flaming region at wavelengths of 4.10 and 4.16  $\mu\text{m}$ , corresponding to the “see to the ground” and CO<sub>2</sub> “blue spike” region. Analyses of the spectra of such fires during both active flaming and lesser intensities were performed as part of these measurements. A sample



Figure 15. Active flames: 4.10  $\mu\text{m}$ .

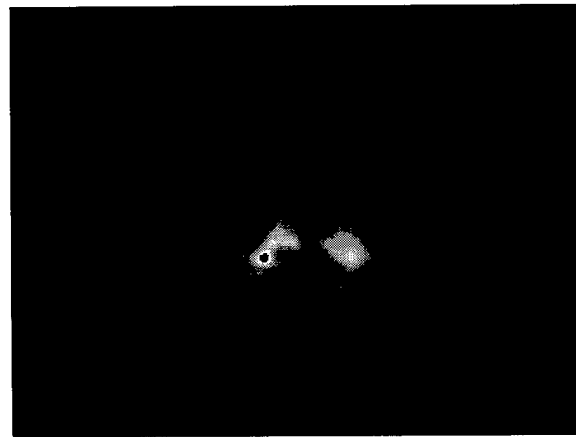


Figure 16. Active flames: 4.16  $\mu\text{m}$ .

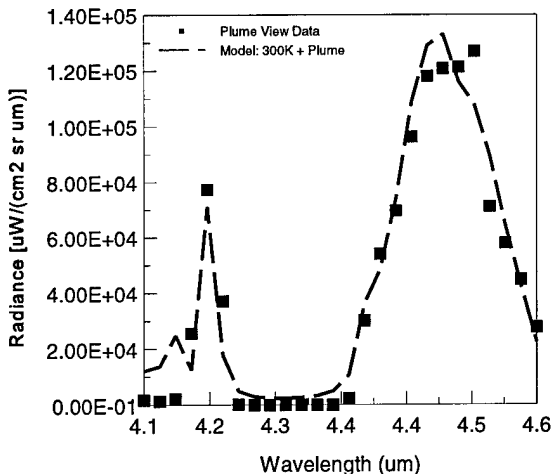


Figure 17. Spectrum of plume region above flames with comparison to MODTRAN simulation of atmospheric transmission coupled with wildfire emission model.

spectrum is shown in Figure 17 for the plume region above the flames. The data is compared to a model of wildfire emission which includes both plume temperature and chemical composition. The MODTRAN atmospheric transmission code is used to convolve the plume emission spectrum with the CO<sub>2</sub> 4.3 µm band absorption. The most notable feature of the model is the inclusion of combustion generated N<sub>2</sub>O in the plume emission signature. The N<sub>2</sub>O levels used in the model agree well with measurements made via grab samples over a range of wildfires and test burns.

Prototype LWIR Imaging System

We have extended the AIRIS concept into the LWIR region through the use of HgCdTe focal planes. The characteristics of the tunable LWIR filter module for this region are shown in Figures 18 and 19. In Figure 18 an FTIR is used to record the transmission spectrum of the étalon in the LWIR. The mirror set used in the interferometer is optimized for the 10 to 14.5 µm region. The spectrum clearly shows the transmission of two orders centered at 10.4 and 12.3 µm, (m=3 and m=2, respectively) establishing a free spectral range of ~2 µm. A detailed examination of the spectral lineshape (Figure 19) shows a good fit to an Airy function with a FWHM of 7 cm<sup>-1</sup>. The challenge in operating an LWIR imager is the selection of a suitable focal plane and the management of self

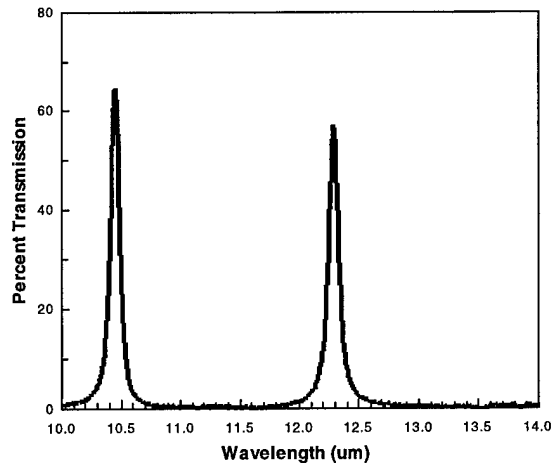


Figure 18. Transmission spectrum of interferometer in LWIR showing 2 orders and establishing the FSR to be ~2 µm. The peak transmission in both orders is ~60%.

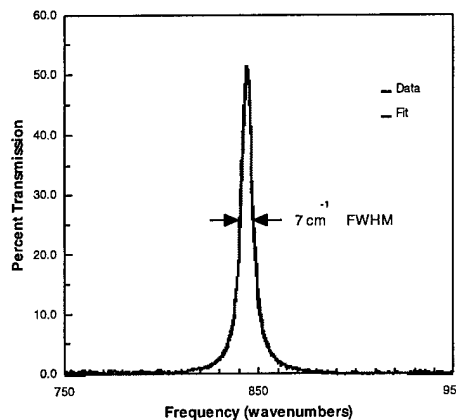


Figure 19. Spectral resolution of LWIR low-order interferometer system with fit to Airy function.

radiance in the optics. To date we have employed a small format HgCdTe array coupled to optical scanners to sample a wide FOV with modest (17 mrad) spatial resolution

The optical layout of PSI's LWIR imaging system is shown in Figure 20. The device utilizes a mechanical chopper and eight channel lock-in amplifier for monitoring the signal from a 2x4 HgCdTe array. The far field scene is constructed as a 48x48 pixel image by rastering the pair of scanning galvo mirrors over 288 discrete positions.

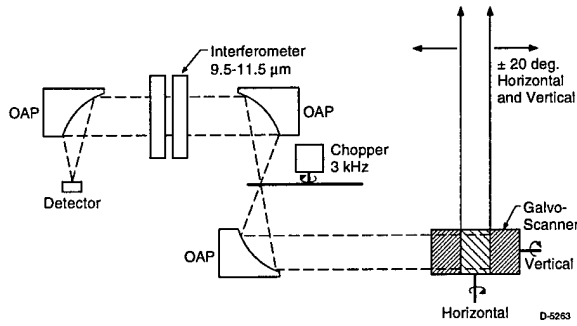


Figure 20. LWIR imaging interferometer configuration employing off-axis parabolic reflectors as focusing elements and a mechanical chopper for improved noise rejection.

We have used the LWIR system to detect sulfur hexafluoride ( $\text{SF}_6$ ) plumes in the laboratory and in the field. The absorption spectrum of  $\text{SF}_6$  in the 10 to 11.5  $\mu\text{m}$  region, measured using the LWIR imaging system and a temperature drop of 5°C between the reference blackbody and the gas, is shown in Figure 21. The location of an optically thin  $\text{SF}_6$  plume in a cluttered scene is accomplished using two-band

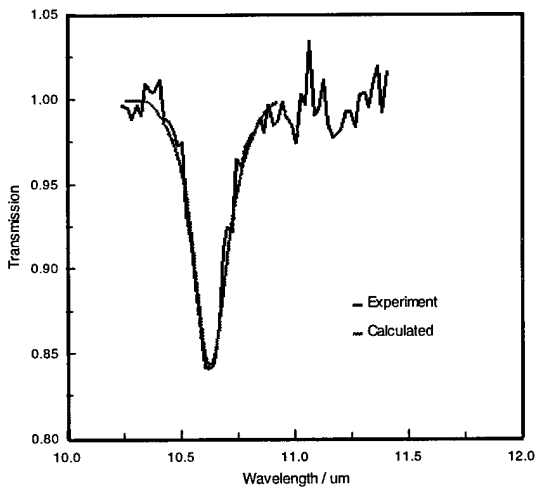


Figure 21.  $\text{SF}_6$  transmission through 10 cm path flow cell at 8 ppm-m concentration and 5 °C temperature drop between gas and reference blackbody.

correlation analysis of scene radiance in the  $\text{SF}_6$  absorption band, 10.55  $\mu\text{m}$ , with the scene radiance at an “out of band” wavelength, 10.85  $\mu\text{m}$  (Figure 22). This approach identifies the location of the the  $\text{SF}_6$  gas flow cell in Figure 23 ( $\text{SF}_6$  line density = 20 ppm

meters) and a plume released in the field, Figure 24. A visible image of the field release site is shown in Figure 25. Details of the LWIR chemical plume imaging experiments will be available in a forthcoming publication.

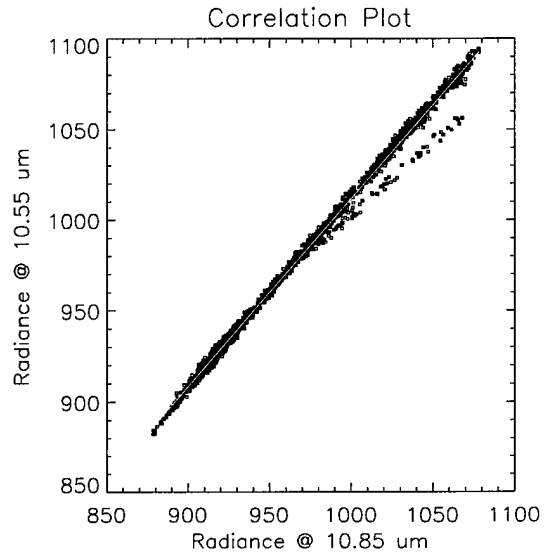


Figure 22. Correlation plot of in-band vs. out-of-band images of a scene containing an  $\text{SF}_6$  flow cell. Pixels exhibiting  $\text{SF}_6$  absorption fall below the primary vector.

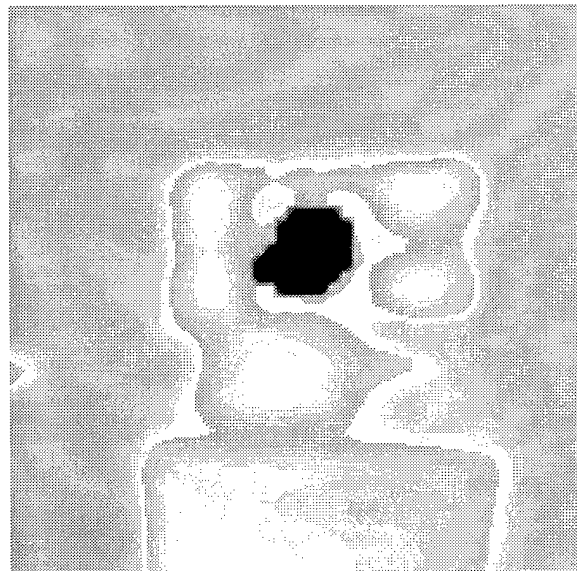


Figure 23. Image at 10.55  $\mu\text{m}$  with location of  $\text{SF}_6$  vapor as identified by two band correlation analysis.  $\text{SF}_6$  location identified by black pixels.

Acknowledgments

The development of the basic *AIRIS* LWIR MWIR technology was funded by BMDO under Contract F30602-94-C-0057 with U.S. Air Force Rome Laboratory. The MWIR imaging effort is funded under contract with the USAF Phillips Laboratory under contract F19628-93-C-0131. Recent development efforts on the LWIR imaging system were funded by the U.S. Army Night Vision and Electronic Sensors Directorate under Phase I SBIR contract, DAAB07-97-C-G006. The authors would like to thank Steve Lipson and Pete Armstrong at PL/GPO for their assistance with MWIR data acquisition and analysis. Finally, PSI would like to acknowledge the assistance of the Armament Directorate of Wright Laboratories (Eglin AFB) and Ron Rapp for the use of *AIRIS-DF* under a bailment agreement.



Figure 24. Spatial distribution of SF6 in outdoor release identified by two-band correlation analysis. Note several "false alarms" at top of scene away from release point.



Figure 25. Outdoor plume imaging configuration. Gas is released from black pipe in the center of the scene.